Multiphysics simulations of nanoarchitectures and analysis of germanium core-shell anode nanostructure for lithium-ion energy storage applications

Multiphysics simulations of nanoarchitectures and analysis of germanium core-shell anode nanostructure for lithium-ion energy storage applications

T Clancy[1], J F Rohan[1]

[1]Tyndall National Institute, University College Cork, Lee Maltings, Cork, Ireland

Email: james.rohan@tyndall.ie

Abstract. This paper reports multiphysics simulations (COMSOL) of relatively low conductive cathode oxide materials in nanoarchitectures that operate within the appropriate potential range (cut-off voltage 2.5 V) at 3 times the C-rate of micron scale thin film materials while still accessing 90% of material. This paper also reports a novel anode fabrication of Ge sputtered on a Cu nanotube current collector for lithium-ion batteries. Ge on Cu nanotubes is shown to alleviate the effect of volume expansion, enhancing mechanical stability at the nanoscale and improved the electronic characteristics for increased rate capabilities.

1. Introduction

Portable personal electronic devices rely on batteries for energy storage and operation. Energy provision and storage are well recognised issues for integrated energy storage on chip as the device dimensions decrease, more functionality is added or devices become more autonomous. Lithium-ion batteries are a mature technology and have a high gravimetric and volumetric capacity, which makes them a leading contender for integration with microelectronic devices. Thin-film solid state batteries are being developed for such devices as they have excellent cycle life and can be processed on silicon substrates. The solid state electrolyte ensures that they are intrinsically safe and utilize standard packaging and fabrication processes. In thin-film solid state batteries the cathode thickness is limited to micrometers (<5μm) in a 2D geometry due to the low conductivity and slow transport of ions in the solid state materials. Current commercial thin-film solid state batteries are appropriate for some uses but do not meet the need for developing applications that require more energy and power per area. To meet this increased energy and power density demand, nanoarchitectures and higher specific energy electrode materials need to be developed for lithium-ion batteries.

The geometry and size of the electrodes play an important role in the electrochemical reaction and ion transport in a lithium battery. 3D architectures allow for more electrode surface area to be in direct contact with the electrolyte and theoretically increase the power density. Advances in micro and nano fabrication techniques have allowed for more creativity in battery design. Multiphysics simulations using mathematical models to describe the electrochemical reactions in 2D and 1D porous lithium-ion batteries were first developed by Newman et al. [1]. The Li^+ ion transport in the active material and electrolyte are modeled using Fick's second law and concentration solution theory respectively. Recent works have used Newman's models and applied them to 3D nanoarchitectures to gain insight into the electrochemical reactions [2].

3D nanoarchitectures have also been shown to alleviate the effect of volume expansion, enhancing mechanical stability at the nanoscale [3]. High capacity anode materials such as Si (theoretical capacity 4200 mAh/g) and Ge (1623 mAh/g) are now realistic replacements for the conventional graphite anode (372 mAh/g). Both materials undergo a volume expansion of up to 300% which causes low cycle life in its bulk state due to delamination from the current collector. Ge has many advantages over Si as an anode material for high power applications with 400 times higher rate of Li^+ diffusion at room temperature and 10,000 times the electrical conductivity [4, 5]. They both have a natural oxide on the outermost layer which results in the formation of an inactive solid electrolyte interface (SEI) during the first charge causing a lower coulombic efficiency [6]. Reported 3D geometries of Ge electrodes to date have been nanowires [7], nanotubes [8] and direct deposition onto the 3D current collector [9].

In this work, multiphysics simulations based on COMSOL modules to compare relatively low conductive cathode oxide materials in solid state thin-film micro, nanowire and core-shell nanowire battery geometries. The aim is to gain an insight on the affect the geometry has on battery performance. This work also focuses on the improving the performance of a Ge electrode as an anode material for lithium-ion batteries. The method used DC sputtering of the Ge onto a Cu nanotube array that acted as a current collector. Initial testing of this Cu nanotube core/Ge shell anode array has shown excellent cycle stability and rate capability.

2. Multiphysics simulations

The multiphysics simulations using COMSOL software are based on standard thin-film solid state lithium-ion battery materials: $LiCoO_2$ cathode, Li metal anode and a 1M electrolyte. Non-porous electrodes are used so only Li^+ ion transportation through the electrode/electrolyte boundary areas is considered. The discharge current is measured in C-rate where 1C is a current required to fully discharge the battery in 1 hour.

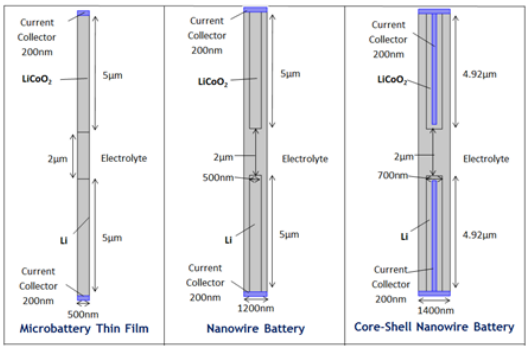

Figure 1. Microbattery thin-film, nanowire battery and core-shell nanowire battery geometries used in simulations.

COMSOL lithium-ion battery and transport of diluted species modules are used to model the thin-film solid state lithium-ion battery. These modules use predefined mathematical equations that are based on the work of Newman [1]. The following assumptions are made:

1. Side reactions are neglected.
2. Volume changes in the electrode are neglected.
3. Atomic movement is described by diffusion where the active material particles are assumed to be one solid non-porous electrode.
4. Diffusion coefficients and conductivities are assumed to be constant within their respective regions in the battery.
5. Electroneutrality is assumed in the electrolyte
6. Anodic and cathodic transfer coefficients are set equal, $\alpha_a = \alpha_c = \alpha = 0.5$, so the exchange current density is calculated from equation (1)

$$i_{0\_pos} = k_{pos}(c_{max} - c)^{\alpha_c} c^{\alpha_a} c_{Li}^{\alpha_a} \quad (1)$$

The geometries used in the simulation are shown in figure 1. All three geometries have an out of plane thickness of 100 µm and volume of 2.5×10^{-16} m^3. The microbattery thin film geometry comprises 5 µm thick electrodes separated by 2 µm of electrolyte. The nanowire battery geometry is composed of a nanowire electrode with a height of 5 µm and diameter of 500 nm, separated by 2 µm and 350 nm either side of the nanowires filled with electrolyte. The base of the nanowire electrodes are connected to 200 nm conductive current collector. The core-shell nanowire geometry is 200 nm diameter conductive nanowire current collector that is covered in electrode material. The electrodes are separated by 2 µm and have 350 nm either side of the electrode which is filled with electrolyte. The

core-shell nanowire electrodes have an overall height and diameter of 4.92 µm and 700 nm respectively.

Table 1. Parameters used in the simulations.

Symbol	Description	Value
c_{Li_init}	Initial Li^+ concentration in electrolyte	1000 mol m^{-3}
c_{init}	Initial Li^+ concentration in cathode	24400 mol m^{-3}
c_{max}	Maximum Li^+ concentration in cathode	51600 mol m^{-3}
D	Diffusion coefficient for Li^+ in cathode	$5x10^{-13}$ m^2 s^{-1}
D_{Li}	Diffusion coefficient for Li^+ in electrolyte	$7x10^{-11}$ m^2 s^{-1}
$conduct_{pos}$	Conductivity of cathode	$1x10^{-6}$ S cm^{-1}
$conduct_{neg}$	Conductivity of anode	$1.05x10^{5}$ S cm^{-1}
$conduct_{electroylte}$	Conductivity of electrolyte	$1x10^{-6}$ S cm^{-1}
k_{pos}	Rate constant charge transfer of cathode	$1.27x10^{-6}$ A m^{-2} (mol m^{-3})$^{-1.5}$
$i_{0\ neg}$	Exchange current density of anode	85 A m^{-2}
t_o	Transference number	0.5
α	Transfer coefficient	0.5
T	Temperature	298.15

The mesh used for this study was an extremely fine edge mesh on the electrode/electrolyte boundaries while the mesh for the remaining geometry was extra fine free triangular mesh. A parametric sweep was used to vary the discharge C-rate. The time dependent study was between 0 and 3600 s with a relative tolerance of 1e-4. The stop condition was timestep <1e-10.

3. Experimental

The design and fabrication of the Cu nanotube core/Ge shell anode is shown in figure 2. Cu nanotubes were fabricated by electrodeposited in 21 mm diameter AAO (Anodised aluminum oxide membranes, Whatman, 60 µm thick, 250-300 nm pore diameter and 10^9 pores cm^{-2}) template with a 700nm Ag seed layer as described in an earlier publication [10]. Briefly, a Cu backing layer was electrodeposited to the Ag-conducting side of the template to give the Cu nanotubes more support once the template was removed. Cu Nanotubes were deposited by using 0.24 M $CuSO_4.5H_2O$ (Sigma Aldrich), 1.8 M H_2SO_4 (Sigma Aldrich), 400 ppm PEG (Sigma Aldrich) and 120 ppm NaCl (Sigma Aldrich) electrolytic bath. A potentiostat (CH instrument 660C) was used to apply a constant current of 40 mA for 900 sec in the two electrode setup with Cu foil as the anode and the AAO template as the cathode. The AAO template was dissolved in a 1M NaOH (Sigma Aldrich) solution for 1 hr, washed with DI water and dried in air. Ge was deposited onto the surface of the Cu nanotube array using a 99.99% pure Ge target (Kurt J. Lesker) and was DC-sputtered (Quorum Q300T D Dual) at a pressure of $1x10^{-2}$ mBar. The sputtering current used was 90 mA for 11 min.

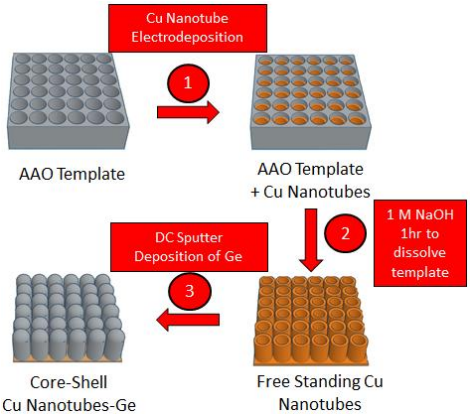

Figure 2. Schematic of the design and fabrication of Cu nanotube core/Ge shell anode. (1) Cu nanotube electrodeposition; (2) AAO template dissolved in 1 M NaOH; (3) DC sputtering of Ge onto the surface of the Cu nanotubes

The structure and the morphology of the samples were analysed (FEI Nova 630 Nano-SEM) coupled with an energy dispersive X-ray (EDX) (Hitachi S4000) and an X-ray powder diffraction (XRD) (Philips PW3710-MPD with Cu K_α radiation, l = 1.54056 Å, at 45 kV (40 mA), and data was analyzed using Philips X'Pert XRD software).

Electrochemical measurements of the Li^+ capacity were performed by cyclic voltammetry (CV) and galvanostatic cycling tests using a potentiostat (Bio-logic VSP) at various scan rates and

discharge/charge currents, respectively. A two electrode cell setup of lithium foil 0.25 mm thick (Sigma Aldrich) acted as counter and reference and the Cu nanotube core/Ge shell anode as the working electrode in 1 M $LiPF_6$ in ethylene carbonate/diethyl carbonate (50:50 volume) (Sigma Aldrich) electrolyte assembled in an argon-filled glove box (M. Braun LABstar Glove Box) with O_2 and H_2O maintained below 0.1 ppm.

4. Results and discussion

The electrochemical activity of the battery geometry was evaluated by the development of concentration profiles and corresponding discharge curves. The potential cut-off is 2.5 V. The COMSOL simulation uses the diffusion coefficient and conductivity values of a solid state electrolyte. The conductivity value of the cathode oxide material is characteristic of a cathode without any conductive additives. Simulated battery discharge capacity at various C-rates for the microbattery thin-film, nanowire and core-shell nanowire geometries are presented in figure 3. The microbattery thin-film curve is characteristic of thin-film solid state batteries due to the internal resistance from the low conductivity of the cathode oxide material and electrolyte. This internal resistance causes a large voltage drop at high discharge currents forcing the potential to drop below the cut-off voltage of 2.5 V. The simulations suggest the implementation of nanoarchitectures such as nanowires and core-shell nanowires for all solid state batteries could increase the discharge rate up to 25C and 30C with a maximum charge/discharge of the cell capacity in 2 minutes.

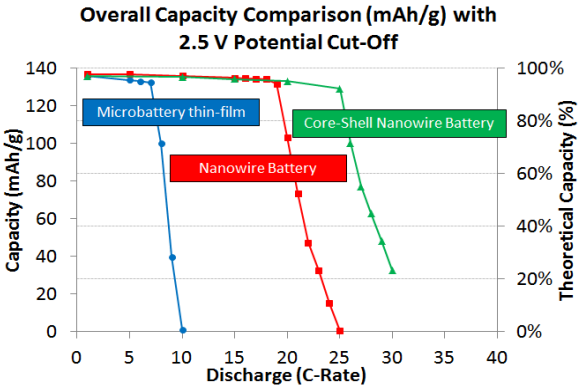

Figure 3. Galvanostatic C-rate discharge comparison for microbattery thin-film, nanowire battery and core-shell nanowire battery geometries.

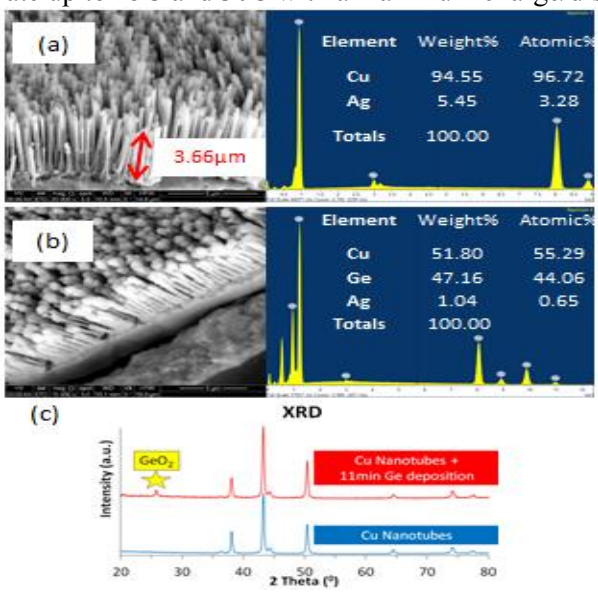

Figure 4. (a) SEM/EDX of electrodeposited Cu nanotubes; (b) SEM/EDX of Ge DC sputtered on Cu nanotube array; (c) XRD of Ge on Cu nanotubes and Cu nanotubes.

Figure 4a is a SEM and EDX image of the electrodeposited Cu nanotubes current collector. The image shows electrodeposited hollow Cu nanotubes, perpendicular to the Ag seed layer and have a smooth surface. The SEM and EDX image of the Cu nanotubes with 11 min DC sputtering of Ge is shown in figure 4b. The EDX confirms the presence of Ge and Cu as the prevalent elements while the SEM illustrates the formation of a uniform layer of Ge on top of the Cu nanotubes from the increase in diameter and rough surface. The XRD analysis shown in figure 4c suggests a natural oxide GeO_2 formed on the surface the Ge. The weight of Ge deposited on the Cu nanotubes that is used for the electrochemical analysis is calculated by measuring the thickness deposited on a planar Cu substrate, the density of Ge 5.323 g/cm^3 and the anode area exposed to the electrolyte in the electrochemical cell.

The electrochemical performance of the Cu nanotubes core/Ge shell was studied by CV and galvanostatic cycling. Figures 5a,b show a CV of cycles 36-40 at a scan rate 0.10 mV/s and the charge/discharge capacities of a range of CVs at different scan speeds vs cycle numbers 1-45 respectively. The cathodic peaks at 0.61 V, 0.31 V and 0.05V during the charging cycling are

associated with the formation of the Li-Ge alloy while the broad anodic peak at 0.49 V is associated to the de-alloying of Li_xGe to Ge. The large initial charge capacity of 2300 mAh/g can be linked to the formation of the SEI layer due to the native oxide of GeO_2 identified from the XRD. The CVs of cycles 36-40 show excellent overlap which indicates little or no degradation in performance. Galvanostatic cycling was performed on the same sample over a range of current. Figure 5c,d shows the galvanostatic cycles 81-85 at a current of 120 µA and the charge/discharge capacities of the galvanostatic cycles performed over a range of currents vs cycle numbers 66-100. The galvanostatic cycles show great reproducibility and Coulombic efficiency above 90%.

The exceptional cycling stability over a range of scan rates and current densities highlights the robustness and advantages associated with the 3D core-shell nanoarchitecture permitting the Ge to expand and contract without detaching from the Cu nanotube current collector.

5. Conclusion

In summary, nanowire and core-shell nanowire battery geometries have shown greater rate capabilities compared to thin film micro-batteries using COMSOL multi-physics simulations. These results indicate that nanowire and core-shell nanowire battery geometries can potentially help meet the demand of for energy and power per unit footprint. Cu nanotube core/Ge shell anode design and fabrication can alleviate the volume expansion during high-rate cycling for lithium-ion batteries.

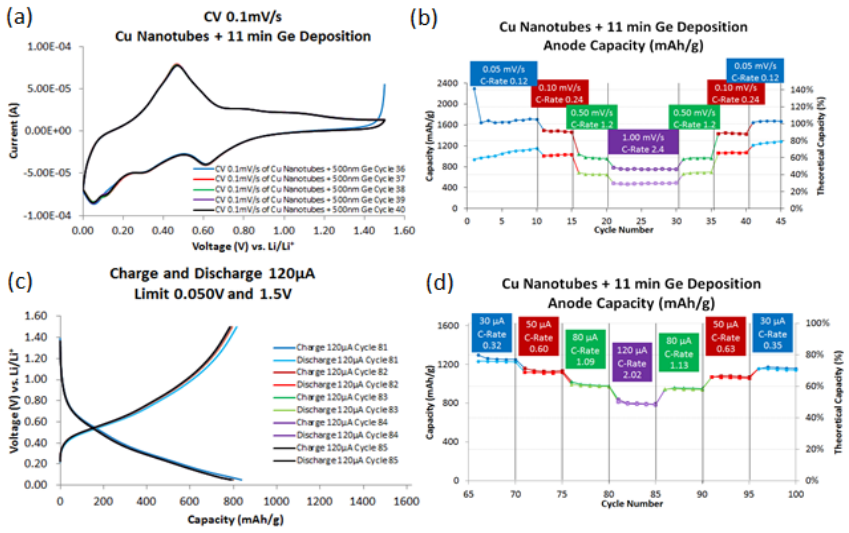

Figure 5. (a) CV at 0.10 mV/s of cycles 36-40; (b) Charge/discharge capacities of CVs vs cycle number; (c) Galvanostatic cycling at 120 µA for cycles 81-85; (d) Charge/discharge capacities of galvanostatic cycles vs cycle number.

Acknowledgments

The authors would like to acknowledge the financial support from SFI Grant number: 12/IP/1722, Nanomaterials design and fabrication for energy storage.

References

[1] Doyle M, Fuller T F and Newman J 1993 *J. Electrochem. Soc.* **140** 1526-33
[2] Zadin V, Kasemagi H, Aabloo A and Brandell D 2010 *J. Power Sources* **195** 6218-24
[3] Hasan M, Chowdhury T and Rohan J F 2010 *J. Electrochem. Soc.* **157** A682-A88
[4] Graetz J, Ahn C C, Yazami R and Fultz B 2004 *J. Electrochem. Soc.* **151** A698-A702
[5] Wang D, Chang Y-L, Wang Q, Cao J, Farmer D B, Gordon R G and Dai H 2004 *J. Am. Chem. Soc.* **126** 11602-11
[6] Seng K H, Park M-h, Guo Z P, Liu H K and Cho J 2013 *Nano Lett.* **13** 1230-36
[7] Kennedy T, Mullane E, Geaney H, Osiak M, O'Dwyer C and Ryan K M 2014 *Nano Lett.* **14** 716-23
[8] Park M-H, Cho Y, Kim K, Kim J, Liu M and Cho J 2011 *Angew. Chem. Int. Edit.* **50** 9647-50
[9] Wang J, Du N, Zhang H, Yu J and Yang D 2012 *J. Mater. Chem.* **22** 1511-15
[10] Chowdhury T, Casey D P and Rohan J F 2009 *Electrochem. Commun.* **11** 1203-06